Microfluidic device concept based on microoscillator dynamics at a liquid–liquid interface

A. Allievi*

Buenos Aires Institute of Technology (ITBA), Microfluidic and Nanofluidic Systems Lab, Department of Mechanical Engineering, Av. Eduardo Madero 399, (C1106ACD) Buenos Aires, Argentina

Abstract

Oscillating microbeams and microplates have been used extensively as sensing components for property detection in fluids. In liquids, their quality factor Q is drastically decreased, thus affecting a microsensor's resolution. To improve the Q-factor, we present a novel concept based on the positive use of surface tension on a mechanical oscillator composed of a microbeam–microplate assembly suspended at a liquid–liquid interface in a microfluidic channel. An analytical model is developed to investigate rotational dynamics of such an assembly. Surface tension effects at the liquid–liquid–solid perimeter line produce responses that are considerably different from those in a single fluid. It is shown that due to surface tension the Q-factor and the response are magnified by orders of magnitude, thus confirming that liquid–liquid interfaces enhance the oscillator's sensitivity. For two liquids the Q-factor varies as $[\sigma_2 - \sigma_1]^{1/2} \times (\mu_2 + \mu_1)^{-1}$ and for a single liquid as $\rho^{1/2} \times \mu^{-1}$, (σ, μ) being surface tension and viscosity, respectively. Microdevice design, actuation and sensing mechanisms, and optimal parameter selection are proposed.

Keywords: Dynamics; Liquid–liquid interface; Surface tension; Microoscillator; Microdevice design; Microfluidics

1. Introduction

The study of fluid–structure interaction of mechanical oscillators in sensor technology has attracted the attention of researchers for over two decades (Hauptmann, 1991). The invention of the atomic force microscope (AFM) (Binnig et al., 1986) encouraged numerous investigations in areas such as dynamic properties of microbeams for sampling surfaces in gases and liquids (Butt et al., 1993; Chen et al., 1994; Walters et al., 1996), measurements of density and viscosity in liquids (Inaba et al., 1993; Oden et al., 1996; Patois et al., 2000), monitoring chemical reactions (Ahmed et al., 2001), cell detection (Yi et al., 2003), and dynamic effects near confining walls (Naik et al., 2003). Among microsensor designs based on microplate dynamics we find concepts based on surface shear oscillations for measuring liquid density and viscosity (Martin et al., 1994; Jakoby et al., 2003), on micromachined diaphragms with piezoelectric thin films (Zhang and Kim, 2003) and on electrothermally excited disk shape structures for chemical and biological applications (Seo and Brand, 2005), to name only a handful of contributions.

*Tel.: +54 11 6393 4800.
E-mail addresses: Alejandro.Allievi@gmail.com, aallievi@itba.edu.ar

Microoscillator-based sensors are particularly attractive for their smaller and less expensive equipment, and for their minute requirements in sample volumes. However, when operating in liquids they share the drawbacks of increased effective mass due to the relatively large viscosity-induced added mass accelerated by the oscillator's motion, and the considerable reduction in quality factor Q due to higher viscous damping. Such decrease in the Q-factor implies that an oscillator's response near the resonant frequency would be weaker, thus making the resonator less sensitive to a given input signal. In order to improve this deficiency in the Q-factor, active feedback control of oscillating cantilevers was proposed (Anczykowski et al., 1998; Tamayo et al., 2001). More recently, the liquid was confined to microchannels inside oscillating microbeams operating in air (Burg and Manalis, 2003), altogether avoiding the operation in a liquid medium.

In this work, we present an alternative, simple and novel concept where surface tension is positively used to increase the quality factor Q of a micromechanical oscillator operating at the interface between two immiscible liquids. We show that such a configuration increases a microoscillator's sensitivity allowing access to useful data with smaller input signals. We develop an analytical model that can be used to tune, analyze and design the proposed configuration, allowing optimal parameter selection for a predefined range of operational conditions and practical purposes. Envisioned added benefits of our concept include the possibility of direct integration into microfluidic systems for real time measurements, a relatively simple and inexpensive microfabrication process flow, and the possibility of parallel analysis of numerous liquid samples.

The remainder of the paper is organized as follows. In Section 2 we derive the equation of motion of the microbeams–microplate assembly along with each of its contributing terms. Section 3 briefly outlines the solution procedure and presents results for various liquid combinations and dimensional parameters of the proposed configuration. Sections 4 and 5, respectively, address microsensor applications and design of the proposed microdevice. Finally, in Section 6 we state our conclusions.

2. Analytical model

Figs. 1(a) and (b) show the schematic representation of a microchannel containing two immiscible liquids of depths d_1 and d_2 separated by an interface assumed of negligible thickness. Each fluid has density, surface tension and viscosity triplets $(\rho_i, \sigma_i, \mu_i)$, with $i = 1, 2$. At the interface of the two liquids, a rigid microplate is suspended from the side walls of the microchannel by means of clamped microbeams, Fig. 2. Without external excitation the two liquids and the microplate remain at rest. In this case, the undisturbed interface is assumed to be a straight horizontal line coinciding with the x-axis and normal to the vertical z-axis. If a pulsating pressure of amplitude P and cyclic frequency ω_p is applied to the right-end wall of the microchannel, it generates an interfacial traveling wave of peak-to-peak height H, circular frequency ω and crest-to-crest wavelength λ. At a location x, the interface elevation is defined as

$$\zeta(t) = \frac{H}{2}\cos(kx - \omega t), \tag{1}$$

where $k = 2\pi/\lambda$ is the wavenumber, t is time, and ω, derived in Allievi (2005), is given by

$$\omega^2 = \left[\frac{2\pi g}{\lambda}(\rho_2 - \rho_1) + \frac{8\pi^3}{\lambda^3}(\sigma_2 - \sigma_1)\right] \times \frac{\tanh(kd_1)\tanh(kd_2)}{\rho_1 \tanh(kd_2) + \rho_2 \tanh(kd_1)}. \tag{2}$$

The dependence of the wave frequency with density and surface tension ratios is shown in Fig. 3. At microscale, unlike with macroscale phenomena, interfacial wave frequency decreases with increasing density ratios and increases with increasing surface tension ratios. Fig. 4 shows the remarkable magnification of wave frequency caused by surface tension at microscale, an effect that becomes negligible at macroscale wavelengths.

In the absence of interfacial waves, the horizontal line $\mathbf{WL}_0$ passing through the center of gravity $\mathbf{G}$ of the microoscillator coincides with the liquids' interface, Fig. 5. In this position, the microoscillator can be considered in equilibrium under the influence of symmetric forces due to surface tension, buoyancy and its own weight. When a sinusoidal interfacial wave train moves along the microchannel, it causes rotational motion of the oscillator from $\mathbf{WL}_0$ to $\mathbf{WL}_1$. In this case, application of the general form of Newton's second law of angular momentum can be written as

$$M^I(\ddot{\theta}, t) + M^D(\dot{\theta}, t) + M^R(\theta, t) = M^F(t). \tag{3}$$

Eq. (3) represents moments due to mass moments of inertia, both liquids' viscous damping effects, restoring effects and inclining moments due to the liquids interface. In the following sub-sections we describe each of these terms for the specific scenario presented in this work. All dimensions correspond to those shown in Figs. 1, 2 and 5.

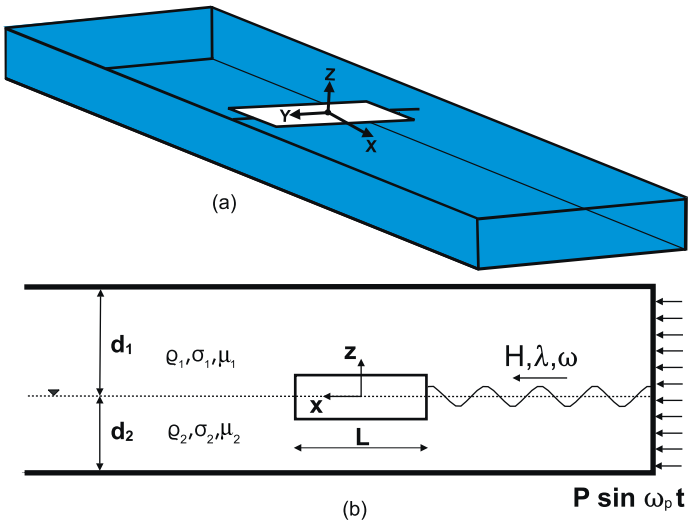

Fig. 1. Microchannel configuration. (a) Three-dimensional view. (b) View along x–z plane at microchannel's mid-width ($y = 0$).

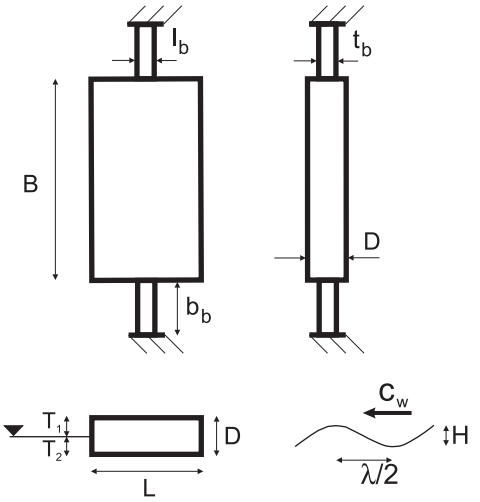

Fig. 2. Top and side views of microplate–microbeam assembly showing dimensional parameters used.

2.1. *Inertia moment* $M^I(\ddot{\theta}, t)$

Re-writing (3) about the y-axis passing through the center of gravity of the microplate gives

$$\sum M = I_{yy}\ddot{\theta}(t), \tag{4}$$

where I_{yy} is the total mass moment of inertia, $\ddot{\theta}(t)$ is angular acceleration and $\sum M$ is the summation of all moments applied to the microplate. The right-hand side of (4) is identical to $M^I(\ddot{\theta}, t)$ in (3). We can expand the expression for I_{yy} as

$$I_{yy} = I^p_{yy} + I^{st}_{yy} + I^{am}_{yy}, \tag{5}$$

where I^p_{yy} is the mass moment of inertia of the microplate, I^{st}_{yy} is the added mass moment of inertia due to both liquids' surface tension, and I^{am}_{yy} is the added mass moment of inertia due to the acceleration of the mass of liquids in contact with the microplate.

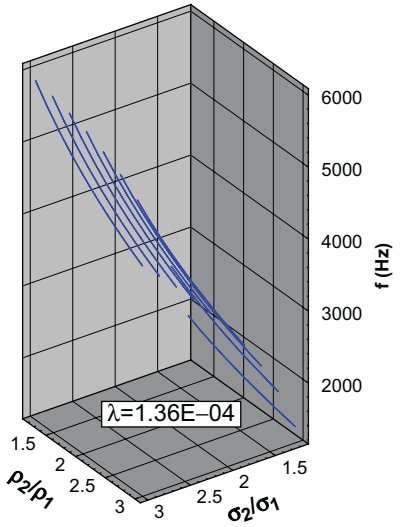

Fig. 3. Interfacial wave frequency as a function of density and surface tension ratios.

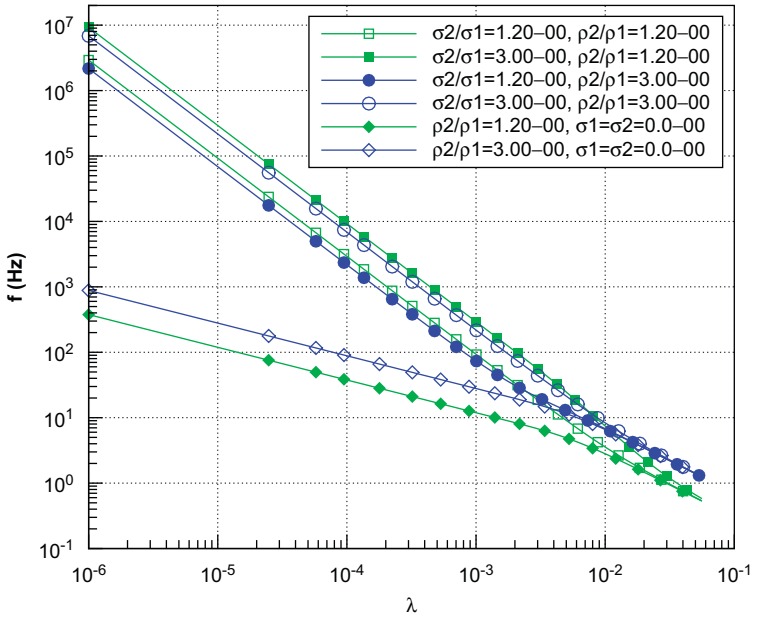

Fig. 4. Interfacial wave frequency as a function of interfacial wavelength in meters.

The expression for I^p_{yy} for rectangular cross-sections is

$$I^p_{yy} = \rho^p LBD\frac{(D^2 + L^2)}{12}, \tag{6}$$

where ρ^p is the density of the microplate material.

The interfacial tension of both liquids at the liquid–liquid–solid perimeter line is responsible for a force similar to that experienced by a Wilhelmy plate in contact with one liquid. Based on the Wilhelmy method used in measuring surface

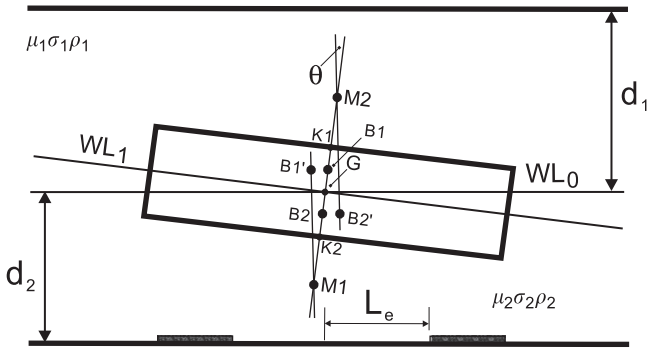

Fig. 5. Microplate rotated cross-sectional side view positioned at liquid–liquid interface. The position of the actuation and sensing electrodes on the lower substrate is shown.

tension, the added inertia due to surface tension at a liquid–liquid–solid interface can be computed as

$$I_{yy}^{st} = 2(\sigma_2 - \sigma_1)(L + B)\frac{(D^2 + L^2)}{12g}, \tag{7}$$

where σ_1 and σ_2 are the surface tensions for each liquid. The term $2(L + B)$ is the perimeter of the plate. A zero contact angle is assumed, limiting the validity of this particular expression to a material design space providing this effect (Rey, 2000). Finally, I_{yy}^{am} can be written as

$$I_{yy}^{am} = \frac{\pi}{256}(\rho_1 + \rho_2)L^4 B, \tag{8}$$

where the underlying assumption is that added inertia due to liquid acceleration around a microplate rotating at an interface can be obtained by halving the value for an infinite fluid if the frequency of oscillation is high.

2.2. Damping moment $M^D(\dot{\theta}, t)$

In the context of microstructures, the squeeze film of the fluid gap under a movable plate in closed proximity to a fixed surface has been identified as the major source of damping (Pan et al., 1998; Veijola et al., 2005). In this work, we compute the effect of squeeze film damping due to the proximity of the upper and lower walls of the microchannel as (Veijola et al., 2005)

$$M^D(\dot{\theta}, t) = M_1^D(\dot{\theta}, t) + M_2^D(\dot{\theta}, t), \tag{9}$$

where

$$M_1^D(\dot{\theta}, t) = \left\{\frac{B[L + 1.65(d_1 - T_1)]^4\mu_1^{\text{eff}}}{15L(d_1 - T_1)^3} + 3.2\mu_1^{\text{eff}}B\sqrt{\frac{L + 2.7D}{d_1 - T_1}}\right\}\left\{\frac{L}{2}\right\}^2\dot{\theta}(t), \tag{10}$$

$$M_2^D(\dot{\theta}, t) = \left\{\frac{B[L + 1.65(d_2 - T_2)]^4\mu_2^{\text{eff}}}{15L(d_2 - T_2)^3} + 3.2\mu_2^{\text{eff}}B\sqrt{\frac{L + 2.7D}{d_2 - T_2}}\right\}\left\{\frac{L}{2}\right\}^2\dot{\theta}(t), \tag{11}$$

and $\dot{\theta}(t)$ is the angular velocity of the microplate. The mean free path of liquids is much smaller than that of gases, typically 1 Å (Kedzierski, 2003), resulting in Knudsen numbers in the range $10^{-3} > K_n > 10^{-6}$. Then the values for effective viscosities μ_i^{eff} in (10) and (11) can be taken as the bulk viscosity coefficient μ_i $(i = 1, 2)$ (Veijola et al., 1995).

2.3. Restoring moment $M^R(\theta, t)$

The moment responsible for the spring term in the ordinary differential equation of motion (3) is the righting moment $M^R(\theta, t)$. It can be written as

$$M^R(\theta, t) = M_g^R(\theta, t) + M_b^R(\theta, t) + M_\sigma^R(\theta, t), \tag{12}$$

where $M_g^R(\theta,t)$ is due to gravitational effects, $M_b^R(\theta,t)$ is due to beams' torsional effect, and $M_\sigma^R(\theta,t)$ is due to surface tension in the liquids.

When tilted to an angle θ, a freely floating microplate resting at the undisturbed interface between two liquids will shift the centers of buoyancy ($\mathbf{B}_1$, $\mathbf{B}_2$) to ($\mathbf{B}_1'$, $\mathbf{B}_2'$). In this new position, the lines of action of the buoyancy forces intersect the original upright vertical line at points ($\mathbf{M}_1$, $\mathbf{M}_2$), Fig. 5. The microplate sustains now a moment $M_g^R(\theta,t)$. When the plate is released from this tilted position, $M_g^R(\theta,t)$ will cause periodic rotation about an axis, which in general does not pass through the center of gravity G. For plates of microscale thickness the distance of such axis to the center of gravity is negligible. Then we can write

$$M_g^R(\theta,t) = g(\rho_2 V_2 \overline{GM_2} - \rho_1 V_1 \overline{GM_1}) \sin(\theta(t)), \tag{13}$$

or for small angular rotations,

$$M_g^R(\theta,t) = g(\rho_2 V_2 \overline{GM_2} - \rho_1 V_1 \overline{GM_1})\theta(t), \tag{14}$$

where V_1 and V_2 are the volumes of liquid displaced by the portions of the microplate at each side of the interface, from which it is clear that in the absence of a liquid–liquid interface there is no restoring moment due to gravitational effects. A geometric analysis of Fig. 5 gives

$$M_g^R(\theta,t) = \frac{gLB}{12}\{\rho_2[L^2 + 6T_2(T_2 - D)] - \rho_1[L^2 + 6T_1(T_1 - D)]\}\theta(t). \tag{15}$$

The moment $M_b^R(\theta,t)$ contributed by the torsional stiffness of each microbeam serving as support for the microplate can be computed for beams of rectangular cross-section as (Timoshenko, 1984)

$$M_b^R(\theta,t) = \frac{\beta l_b t_b^3 G}{b_b}\theta(t), \tag{16}$$

where the numerical factor β depends on the ratio l_b/t_b and G is the beam's shear modulus.

The moment $M_\sigma^R(\theta,t)$ due to surface tension at the liquid–liquid–solid perimeter line is contributed by the imbalance caused by both liquids at the upstream and downstream sides of the microplate. Based on the change of the perimeter at the liquid–liquid–solid interface due to the microplate's rotation, an expression for this moment has been derived as

$$M_\sigma^R(\theta,t) = 2L\left\{\sigma_2 \frac{L^2 + 6T_2(T_2 - D)}{12T_2} - \sigma_1 \frac{L^2 + 6T_1(T_1 - D)}{12T_1}\right\}\left[\frac{1 - \cos\theta(t)}{\cos\theta(t)}\right]\theta(t), \tag{17}$$

which, as expected, vanishes at zero angles of rotation. Eq. (17) shows one of the nonlinear effects introduced by surface tension in the rotational motion of the microplate.

2.4. Forcing moment $M^F(\theta,t)$

So far we have derived the terms that contribute to the left-hand-side of (3) in the absence of interfacial waves. A regular wave train described by (1) has an effective slope at $x = 0$ given by

$$\eta(t) = \frac{\pi H}{\lambda}\sin(\omega t). \tag{18}$$

An analogy with the righting moment (15) yields the wave-induced moment

$$M_w^F(\theta,t) = \frac{gLB}{12}\{\rho_2[L^2 + 6T_2(T_2 - D)] - \rho_1[L^2 + 6T_1(T_1 - D)]\}\eta(t). \tag{19}$$

Surface tension aids the rotational motion by introducing an imbalance as the wave progresses along the microplate. Then, by analogy to (17),

$$M_\sigma^F(\theta,t) = 2L\left\{\sigma_2 \frac{L^2 + 6T_2(T_2 - D)}{12T_2} - \sigma_1 \frac{L^2 + 6T_1(T_1 - D)}{12T_1}\right\}\left[\frac{1 - \cos(\eta(t))}{\cos(\eta(t))}\right]\eta(t). \tag{20}$$

We note here that the underlying assumption in (19) and (20) is that the dimension L of the microplate is small compared to the length λ of the waves. From (19) and (20) we obtain the total righting moment as

$$M^F(\theta,t) = M_w^F(\theta,t) + M_\sigma^F(\theta,t). \tag{21}$$

From expressions (19) and (20) we see that, in view of (2) and (18), when $\sigma_1 = \sigma_2$ and $\rho_1 = \rho_2$, no interfacial waves can be formed, thus leading to a zero forcing function.

3. Solution and numerical results

The series of equations derived in the previous section leads to an ODE of the form

$$a_1\ddot{\theta}(t) + a_2\dot{\theta}(t) + a_3\theta(t) = M(t), \tag{22}$$

that was integrated in time. Table 1 shows the microbeam and microplate dimensions used. Wave conditions and liquid properties are presented in Tables 2 and 3. Simulation runs are uniquely identified by run IDs made by combinations of identifiers listed under *Case* in each table. We have taken the quality factor to be $Q = f_0^{-1}/2\pi(a_3/a_2) = \sqrt{a_3 a_1}/a_2$, and the undamped natural frequency of the oscillator as $f_0 = [1/(2\pi)]\sqrt{a_3/a_1}$.

In order to demonstrate the remarkable increase in Q-factor due to liquid interfaces, we first obtained damped free responses of the system. Initial conditions $(\dot{\theta}^0, \theta^0) = (0.0, 0.05)$ were used. Surface tension, not present in the case of single fluid media, dramatically affected the Q-factor. Response decay rates decrease by orders of magnitude with respect to those in a single liquid. Mathematically, this phenomenon can be confirmed by analyzing the data provided in Table 4 (repeated case IDs imply single liquid). We know that for a single liquid the quality factor Q decreases with increasing values of viscosity. However, unlike single-liquid phenomena, the increase in added inertia due to surface tension offsets viscous damping producing a significant increase of the Q-factor. We note from Table 4 that even at the extreme end of equivalent viscosity (W–OO) where the Q-factor is the lowest, it is still nearly 50 times greater than the single liquid value (O–O).

We now examine the response of the oscillator under the excitation of waves developed at the interface of different liquid–liquid combinations. Initial conditions $(\dot{\theta}^0, \theta^0) = (\dot{\theta}_{t=0}, \theta_{t=0}) = (0.0, 0.0)$ have been used. Interfacial wave conditions used are those identified as MW1, MW2, MW3 and MW4 in Table 2. Fig. 6 shows frequency response curves obtained using a very small wave amplitude of $H/2 = 0.5\,\mu\text{m}$ to assess the response of the oscillator to a very weak input signal. Frequency shifts are clearly observed among all liquid combinations. The bandwidth Δf increases as the quality factor decreases, a fact that has been observed by other investigators (Patois et al., 2000). As derived in the Appendix, the Q-factor variation for two liquids follows $[\sigma_2 - \sigma_1]^{1/2} \times (\mu_2 + \mu_1)^{-1}$ versus single liquid's μ^{-1}, Fig. A1.

It is important to note that an interfacial wave can only develop as a result of some fluid property difference. A single fluid, such as W, has no interface and cannot develop interfacial waves. It is this essential concept that this work attempts to underline, i.e., that liquid property differences can be used to generate an interface and that, at microscale, magnification of the quality factor Q of a microoscillator can be achieved thanks to surface tension effects resulting from such an interface. As a result, sensitivity of a microscale device can be enhanced to measure thermophysical and other interesting properties in liquids.

We have examined the effect of different wave heights on the oscillator's response, Fig. 7. For the smaller height (MW2), the response of the oscillator is perfectly sinusoidal, no second frequency is detected by the FFT of the time record. In this case, the term M_w^F of (19) dominates the forcing function (21). However, when the wave amplitude is increased 10 times (MW3), outstanding increases in peak amplitudes of approximately 136 times for W–B and of 200 times for W–SO1 occur, i.e., response magnifications of over an order of magnitude greater than the increase in excitation amplitude. A second frequency is also now detected by the FFT. Such frequency is contributed by M_σ^F in (20), the nonlinear term associated to the surface tension difference in the liquids. For the smaller wave height, the slope is very small and the term $1 - \cos(\eta(t))$ in (20) is virtually zero. As a consequence the influence of M_σ^F is negligible and (19) dominates the forcing term. Observation of Table 3 shows that $\rho_2 - \rho_1$ is greater for W–B than for W–SO1, resulting in greater M_w^F and angular response. However, when the wave amplitude is increased to MW3, the term $1 - \cos(\eta(t))$ is appreciable and the situation is reversed. In this case, Eq. (20) for W–SO1 is greater than for W–B due to a larger $\sigma_2 - \sigma_1$, leading to greater response amplitude. These results indicate that surface tension enhances the sensitivity of the oscillator and magnifies output signal well beyond that expected from an oscillator operating in a single liquid.

From (2) and Fig. 4, we see that halving the wavelength causes a considerable frequency magnification. Fig. 8 shows the effect on the oscillator's response frequency caused by a shortened wavelength. The wave frequencies are 808.8 Hz for MW1 and 211.4 Hz for MW3. These values are very close to the first frequencies of the time response FFTs (804.7 and 208.6, respectively). An equivalent effect is obtained when varying the microchannel dimensions. Fig. 9 shows the effect on the oscillator's response due to tripling the microchannel's height (Case MW4: 328.9 Hz), effectively increasing the interfacial wave frequency through the multiplication of the $\tanh(kd_i)$ terms in the numerator of (2). Clearly, dimensional parameters can be adjusted for a pre-defined range of operational frequencies.

Table 1
Microbeam and microplate dimensions

Microbeam data (μm)				Microplate data (μm)			
Case	l_b	b_b	t_b	Case	L	B	D
MB1	25	100	25	MP1	50	50	25

Table 2
Interfacial wave conditions

Case	λ (μm)	H (μm)	d_i (μm)	T_i (μm)
$MW0_1$	N/A	0	50	12.5
MW1	500	5	50	12.5
MW2	1000	0.5	50	12.5
MW3	1000	5	50	12.5
MW4	1000	5	150	12.5

Table 3
Liquid properties

Liquid media					
Case	Liquid	Density ρ ($kg\,m^{-3}$)	Kinematic viscosity v ($m^2\,s^{-1}$)	Dynamic viscosity μ ($N\,m^{-2}\,s$)	Surface tension σ ($N\,m^{-1}$)
B	Benzene	0.879×10^3	0.736×10^{-6}	0.647×10^{-3}	28.9×10^{-3}
SO1	Silicon oil 1	0.91×10^3	5.0×10^{-6}	4.55×10^{-3}	19.7×10^{-3}
SO2	Silicon oil 2	0.93×10^3	10.0×10^{-6}	9.3×10^{-3}	20.1×10^{-3}
SO3	Silicon oil 3	0.95×10^3	20.0×10^{-6}	19.0×10^{-3}	20.6×10^{-3}
OO	Olive oil	0.92×10^3	91.3×10^{-6}	84.0×10^{-3}	32.0×10^{-3}
W	Water	1.0×10^3	1.0×10^{-6}	1.0×10^{-3}	72.8×10^{-3}

Table 4
Natural frequency, quality factor and ODE coefficients from Eq. (22) ($t = 0$) as a function of equivalent viscosity $(\mu_2 + \mu_1)/2$, equivalent density $(\rho_2 + \rho_1)/2$ and surface tension difference $\sigma_2 - \sigma_1$

Run ID: MB1, MP1, $MW0_1$							
Case	$\frac{\mu_2 + \mu_1}{2} \times 10^3$	$\frac{a_2}{a_1}$	$\sigma_2 - \sigma_1$	$\frac{a_3}{a_1}$	$\frac{\rho_2 + \rho_1}{2}$	f_0	Q
W–B	0.8235	2.1215	0.0439	2.9165×10^{11}	939.5	8.5951×10^4	254 557
W–SO1	2.775	5.9119	0.0531	2.4118×10^{11}	955	7.8162×10^4	83 070
W–SO2	5.15	11.055	0.0527	2.4301×10^{11}	965	7.8457×10^4	44 592
W–SO3	10.0	21.671	0.0522	2.4534×10^{11}	975	7.8832×10^4	22 856
W–OO	42.5	117.79	0.0408	3.1377×10^{11}	960	8.9151×10^4	4755
B–B	0.647	1093.7	0.0	1.9137×10^{14}	879	2.2017×10^6	12 648
W–W	1.0	1686.1	0.0	1.9088×10^{14}	1000	2.1989×10^6	8194
SO1–SO1	4.55	7686.4	0.0	1.9125×10^{14}	910	2.2010×10^6	1799
SO2–SO2	9.3	15 704	0.0	1.9116×10^{14}	930	2.2005×10^6	880
SO3–SO3	19.0	32 070	0.0	1.9108×10^{14}	950	2.2001×10^6	431
OO–OO	84.0	141 870	0.0	1.9121×10^{14}	920	2.2008×10^6	97

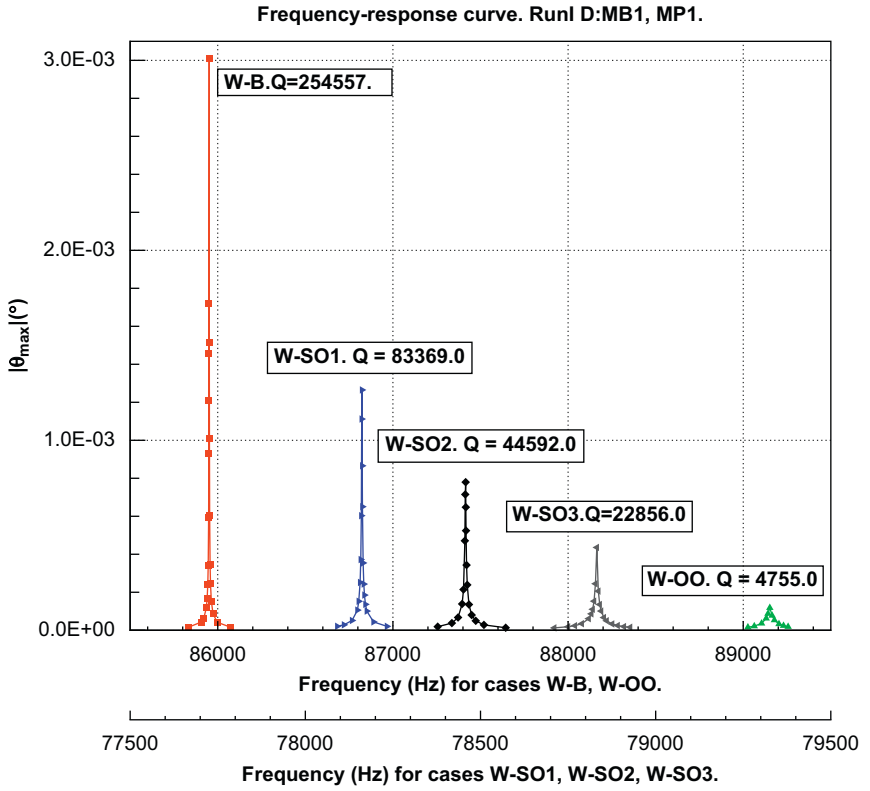

Fig. 6. Frequency–response curves for various liquid combinations and variation of Q-factor with thermophysical properties of the liquids.

4. Applications in microsensing technology

In previous sections we have presented and modeled the physical concepts that lead to improving the sensing capacity of a microsensor operating in liquids. In this section, we introduce two specific scenarios where the proposed concepts can be applied to sensing technology. In this manner, we attempt to simulate the operational principles of the proposed microdevice.

4.1. Fluid property measurements (ρ, σ and μ)

From the decay response of the microoscillator we can obtain its natural frequency in the liquid–liquid medium in which it operates. First and second derivatives of the actual decay response curve provide time domain records for angular velocity and acceleration, respectively. Using a "seed" liquid such as deionized water whose thermophysical properties (ρ_2, σ_2, μ_2) are known, the properties of the other liquid can be obtain as follows. For a given time $t = t_1$ where $\dot{\theta}(t = t_1) = 0$ in the angular velocity time record, we can obtain corresponding values of $\theta(t = t_1), \ddot{\theta}(t = t_1)$. Introducing these values into (22), we find a homogeneous algebraic equation with two unknowns (ρ_1, σ_1). Note that $\dot{\theta}(t = t_1) = 0$ implies a zero damping term and viscosity μ_1 drops out of the algebraic equation.

The second equation can be written by exciting the microoscillator at the natural frequency previously found. Differentiation of such resonance record, provides peaks $\theta(t = t_2)$, $\ddot{\theta}(t = t_2)$ at a given time $t = t_2$. Such values will correspond with zero values of (19) and (20) ($\eta(t = t_2) = 0$) as well as $\dot{\theta}(t = t_2) = 0$. Introducing these values into (22) provides the second equation. Solving the system provides the pair (ρ_1, σ_1). Finally, the original decay record can be used to write a third algebraic equation using non-zero values $\dot{\theta}(t_3)$, $\ddot{\theta}(t_3)$, $\theta(t_3)$. From this we compute μ_1.

4.2. Interfacial wave detection (ω, H and λ) and ambient micropressure measurement

Under the assumption $\lambda \gg L$, the frequency of the forced response record of the oscillator matches that of the excitation frequency with relatively high accuracy. Therefore, FFT of the forced oscillation record of

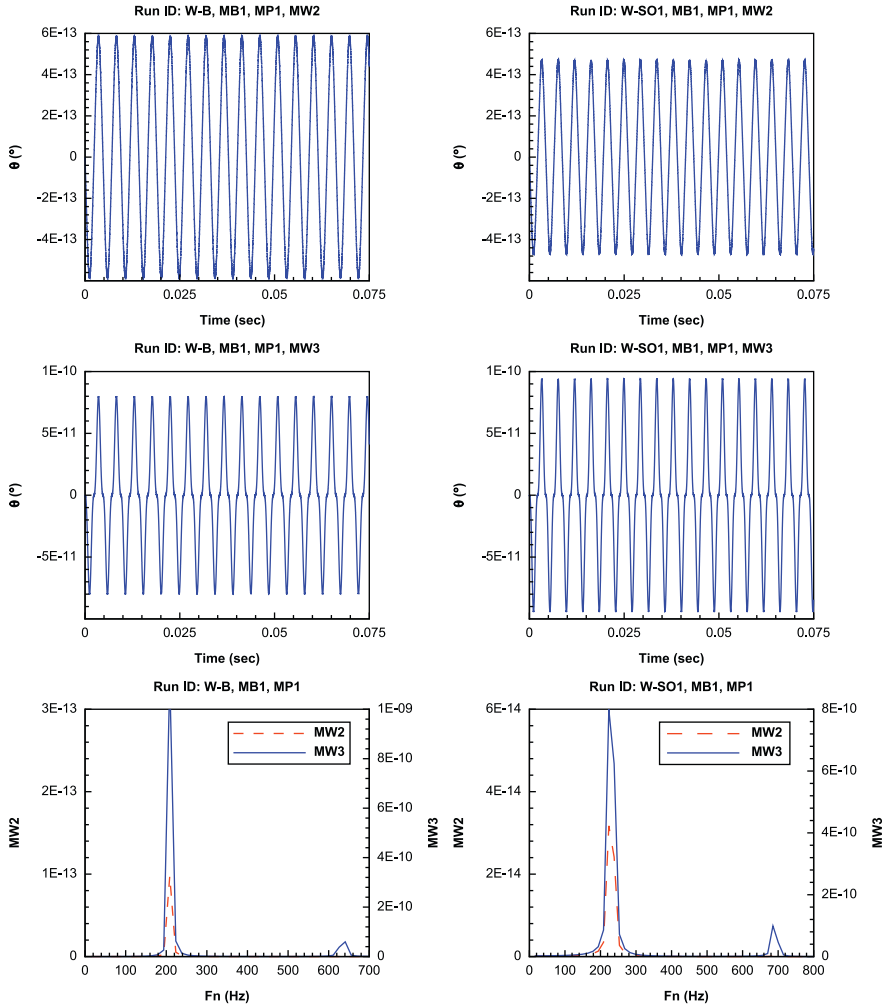

Fig. 7. Effect of interfacial wave height on damped forced response.

the microoscillator provides the frequency of the exciting interfacial wave. Using this response record, a fourth algebraic equation can be written with non-zero values $\ddot{\theta}(t_4)$, $\dot{\theta}(t_4)$, $\theta(t_4)$. With Eq. (18) and the liquid properties obtained in the previous section, this algebraic equation together with (2) yield the height H and length λ of the interfacial wave.

It is possible to compute the deflection of the right-wall of the microchannel and the magnitude of the fluctuating micropressure responsible for the formation of interfacial waves of predetermined characteristics. As derived in Allievi (2005), the ambient fluctuating pressure on the right end causing the interfacial wave of height H and length λ can be computed as

$$P = \frac{6EI}{d^5} \frac{H}{\tanh\left(\frac{2\pi}{\lambda}\mathrm{d}\right)}, \tag{23}$$

where E is the wall's Young's modulus of elasticity and I is its cross-sectional area moment of inertia. We note that $d = d_1 = d_2$ has been assumed.

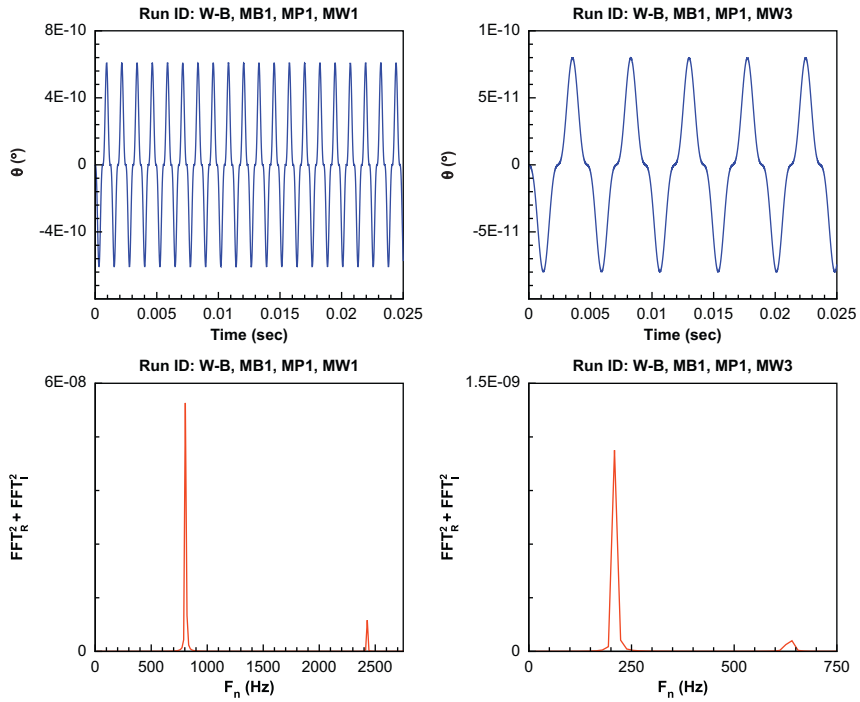

Fig. 8. Effect of interfacial wavelength on damped forced response.

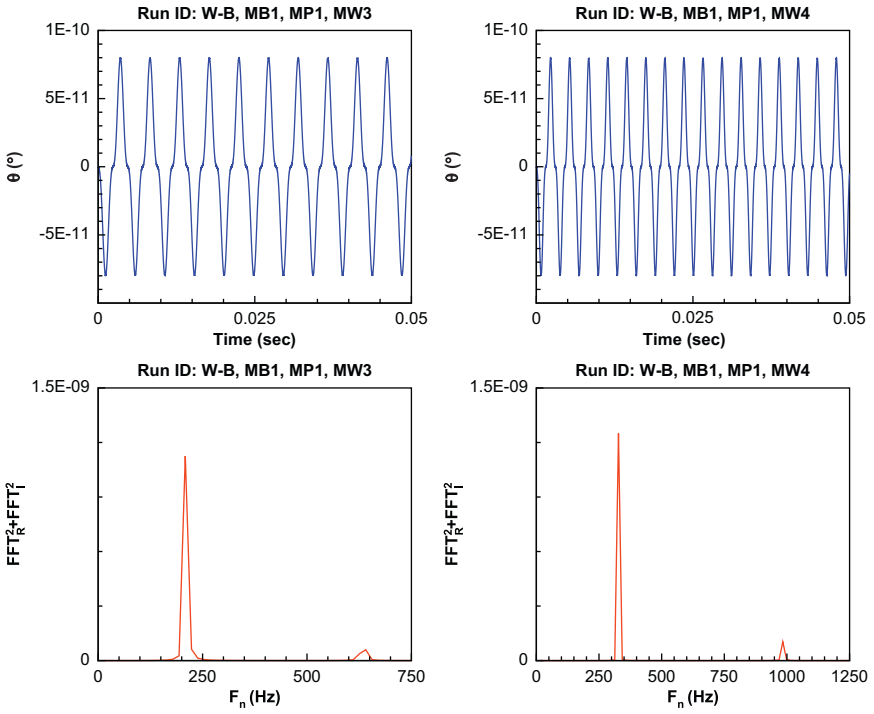

Fig. 9. Effect of microchannel depth on damped forced response.

5. Microdevice design

5.1. General design considerations

In this section, we introduce an engineering design of the proposed microdevice and recommend a strategy for optimal parameter selection. Fig. 10 shows exploded isometric and various views of the proposed microdevice. Lower and upper glass chambers house peristaltic pumps that ensure symmetric pumping of equal volumes for both liquids. This guarantees simultaneous filling of the microchannel regions above and below the microplate. Circular piezoelectric disks are glued to the outside glass membranes of each of the chambers. Each disk is actuated peristaltically by the application of an electric voltage causing the glass membrane to bend downwards (Van Lintel et al., 1988). When the voltage is removed, the membrane returns to its originally flat configuration. For a description of controlling voltages, cycle frequency, number of discs, pumping rates and general operating principles of peristaltic pumps the reader is directed to Smits (1990).

Each of the pump chambers is bonded to the substrates containing the etched microchannel's lower and upper regions. In these substrates, liquid inlets are etched immediately below and above the center point of the microplate. These inlets are in turn positioned immediately above and below the center points of each of the central piezoelectric disks. The upper and lower substrates are to be made of Corning 1737F glass. Separation of microchannel surfaces from pump chambers ensures that moving deformable surfaces are avoided in the microchannel regions where flat surfaces are required, particularly in the neighborhood of the electrodes. The microplate–microbeam assembly as well as the electrodes are made of platinum due to its chemical inertness and good electrical characteristics.

There are two electrodes used in the design shown in Fig. 10. These are to be made of Pt deposited using evaporation techniques on patterns produced photolithographically on the Corning 1737F glass (Chen et al., 2004). One electrode is used as an actuator to rotate the microplate to a predefined angle of tilt. The other electrode is used to capacitively sense the rotation of the microplate, with capacitance increasing as the plate approaches the electrode and decreasing as it

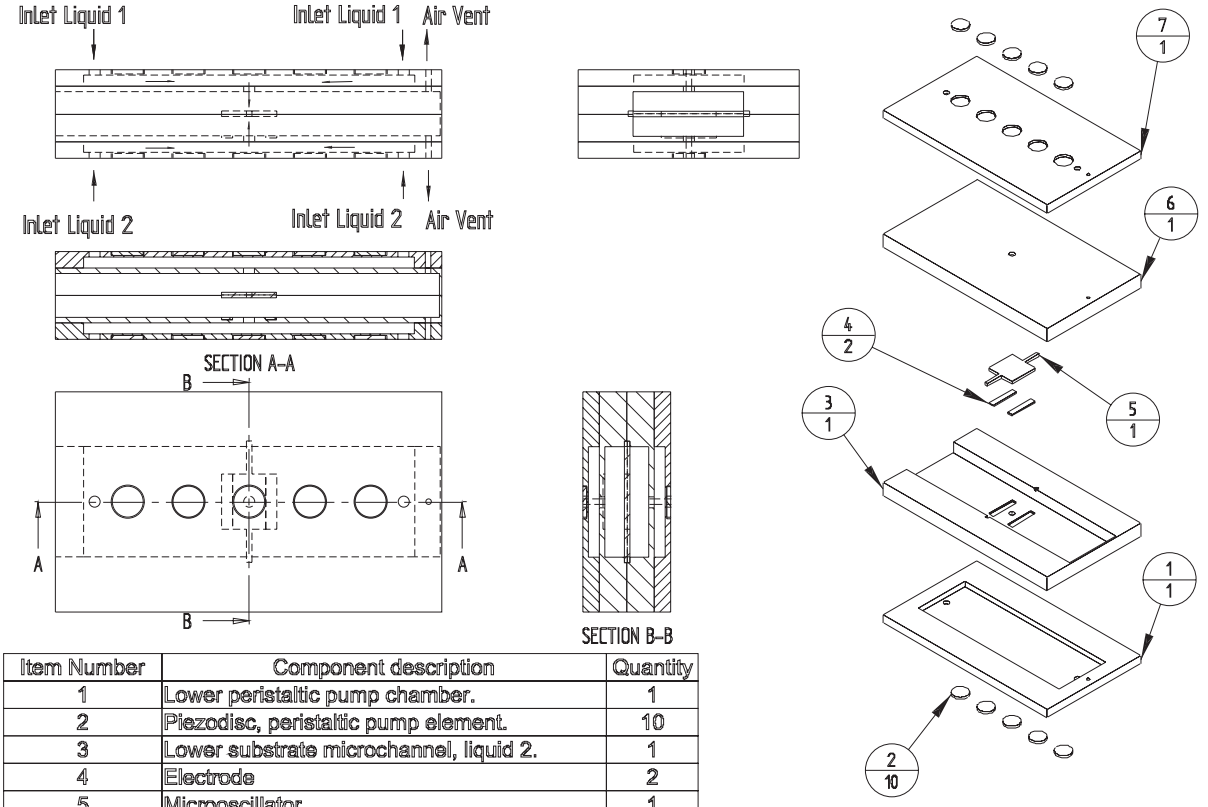

Item Number	Component description	Quantity
1	Lower peristaltic pump chamber.	1
2	Piezodisc, peristaltic pump element.	10
3	Lower substrate microchannel, liquid 2.	1
4	Electrode	2
5	Microoscillator	1
6	Upper substrate microchannel, liquid 1.	1
7	Upper peristaltic pump chamber, liquid 1.	1

Fig. 10. Exploded isometric and various views of the microdevice.

moves away from it. Design, fabrication and characterization of such an arrangement in the context of microcantilevers has been reported in Li et al. (2006). Detailed description of the circuitry for actuation and capacitive sensing of the proposed microbeam–microplate assembly as well as for microdevice fabrication and testing are to be reported in a future publication.

5.2. *Optimal parameter selection*

In Section 4.1 we mentioned that the natural frequency of the device can be obtained from a decay response curve. However, in order to produce such a curve we need to provide a mechanism to tilt the microplate to a predefined angle. Such an operation is achieved by electrostatic means through one of the electrodes at the bottom of the microchannel. In our case, the microplate and the electrodes are positioned very close to each other and the angles of tilt are expected to be very small. Therefore, the electric field at any point in between the microplate and an electrode can be approximated by that corresponding to two parallel plates. Then, it can be shown that the electrostatic moment M_e required to tilt the microplate to a desired angle of actuation θ_a is given by

$$M_e = \frac{\varepsilon V_a^2 B}{\sin^2\theta_a}\left\{\ln\left|\frac{d_2 - \frac{D}{2} - \frac{L}{2}\sin\theta_a}{d_2 - \frac{D}{2} - L_e\sin\theta_a}\right| + \frac{d_2 - \frac{D}{2}}{d_2 - \frac{D}{2} - \frac{L}{2}\sin\theta_a} - \frac{d_2 - \frac{D}{2}}{d_2 - \frac{D}{2} - L_e\sin\theta_a}\right\}, \tag{24}$$

where V_a is the voltage applied between the microplate and the electrodes, ε is the permittivity of the lower liquid and L_e is the distance of the electrode's inner edge from the center of the microplate, Fig. 5. In actuation mode, the electrostatic moment M_e is opposed by the buoyancy restoring moment (15), the beam torsional moment (16) and surface tension restoring moment (17). Then the expression

$$M_e(\theta_a, 0) + M_g^R(\theta_a, 0) + M_b^R(\theta_a, 0) + M_\sigma^R(\theta_a, 0) = 0 \tag{25}$$

can be used to select optimal parameters based on predefined operational conditions.

In order to minimize possibilities of ionization of the lower liquid, this is chosen to be deionized water and the actuation voltage is taken as $V_a = 1.3$. Note that such low voltage would allow for the use of simple batteries for the

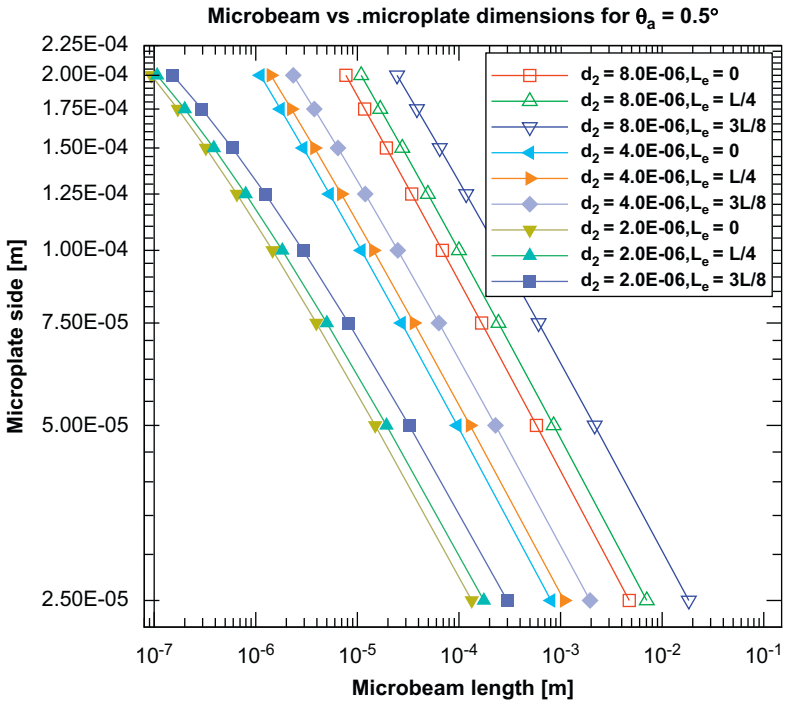

Fig. 11. Required microbeam dimensions for square ($L = B$) microplate actuation to $\theta_a = 0.5^\circ$ as a function of lower liquid depth d_2 and electrode size ($V_a = 1.3V$, $l_b = t_b = D = 1\,\mu\text{m}$). All dimensions are in meters.

actuation step of the microdevice, a feature that would be particularly attractive in hand-held devices. We also restrict ourselves to microplates of square shapes. Under these premises, we can obtain dimensions for the microbeams vs microplate dimensions as a function of the lower microchannel's depth, Fig. 11. This figure allows for the optimal selection of both microplate and microbeam dimensions, which unequivocally determine the width of the microchannel, as a function of the microchannel's depth.

6. Conclusions

A model of the tilt dynamics of a mechanical microoscillator placed at the interface of two immiscible liquids has been presented as a concept where surface tension is positively used to enhance the quality factor. Free damped response of such microoscillator shows a dramatic increase in the Q-factor over the values observed in a microoscillator functioning in a single liquid. Such increase in the Q-factor follows $[\sigma_2 - \sigma_1]^{1/2} \times (\mu_2 + \mu_1)^{-1}$ as opposed to $\rho^{1/2} \times \mu^{-1}$ for a single liquid. When the microoscillator is excited by interfacial waves with very low amplitudes, density dominates the forcing function and a single frequency is visible in the FFT of the response time-records. At higher wave amplitudes, a second frequency appears which is associated with the difference in surface tension of the two liquids. At these higher amplitudes (and wave slopes), a surface tension-dominated nonlinear effect causes magnification of the response of orders of magnitude greater than the increase in the excitation amplitude. Therefore, surface tension can be used to magnify Q-factor and sensitivity of an oscillator allowing sensing with weaker input signals.

A microdevice to implement the proposed concept has been presented, together with a strategy for optimal parameter selection for the microplate–microbeam assembly and for the microchannel dimensions. It has been shown how the microdevice can be used in the design of multi-property microsensor technology for measurement of thermophysical properties in liquids, of wave features at a liquid–liquid interface and of ambient micropressure fluctuations at the boundary of a microchannel. An added benefit of the proposed configuration is direct integration into microfluidic systems for real time measurements of, for instance, mass of biospecies that attach to the upper side of the microplate if this were to be functionalized by deposition of another material. The proposed concept also offers the possibility of massive parallelization for analysis of different liquid samples, together with a relatively simple and inexpensive microfabrication process flow.

Acknowledgment

The author gratefully acknowledges access to facilities provided by Dr. David Juncker from McGill University's Micro & Nano BioEngineering Lab. The assistance of Argentina's CNEA-CAC MEMS Group and of Programa RAICES of Secretaría de Ciencia, Tecnología e Innovación Productiva through grant *Dr Cesar Milstein* is greatly appreciated. The author also thanks one referee's insightful comments to clarify and improve the original manuscript.

Appendix

Here we derive the relationships between the quality factor Q and the fluid thermophysical properties for microchannels with one liquid and with two liquids. These expressions are found by considering the leading terms in the expressions that make up the terms a_1, a_2 and a_3 in (22). To simplify the analysis we assume $B = L$, $T_1 = T_2 = D/2$ and $d_1 = d_2$.

For two liquids in a microchannel, an order of magnitude analysis of a_1, a_2 and a_3 results in

$$a_1 = C_1(\sigma_2 - \sigma_1), \quad a_2 = C_2(\mu_1 + \mu_2), \quad a_3 = C_3$$

and the quality factor Q becomes

$$Q_{2L} = C_{2L}\,[\sigma_2 - \sigma_1]^{1/2} \times (\mu_2 + \mu_1)^{-1},$$

where C_1, C_2, C_3 and C_{2L} are considered constants due to their independence from fluid properties.

For only one liquid in the microchannel, $\sigma_2 - \sigma_1 = 0$, $\rho_1 = \rho_2 = \rho$ and $\mu_1 = \mu_2 = \mu$. An order of magnitude analysis of a_1, a_2 and a_3 leads to

$$a_1 = D_1\rho, \quad a_2 = D_2\mu, \quad a_3 = D_3.$$

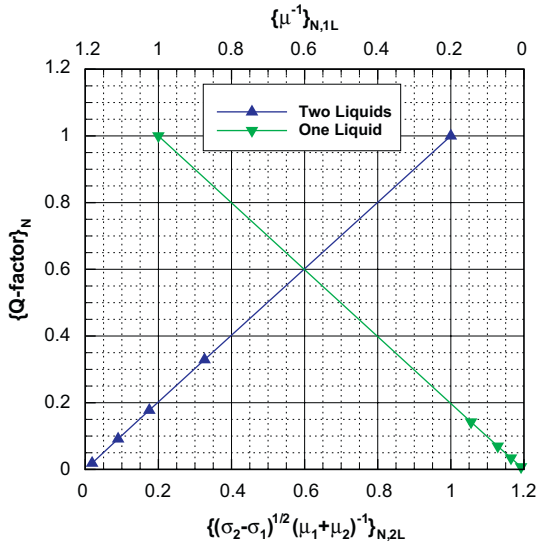

Fig. A1. Variation of Q-factor with liquid thermophysical properties.

The quality factor Q then becomes

$$Q_{1L} = D_{1L}\ \rho^{1/2} \times \mu^{-1},$$

where D_1, D_2, D_3 and D_{1L} are again independent from fluid properties. It should be pointed out that, for the liquids used in this work, the variation of Q_{1L} can simply be taken as $D_{1L}\ \mu^{-1}$. This is clearly seen in Fig. A1, where the N subscript implies a variable normalized by its own maximum value.

References

Ahmed, N., Nino, D., Moy, V., 2001. Measurement of solution viscosity by atomic force microscopy. Review of Scientific Instruments 72 (6), 2731–2734.

Allievi, A., 2005. Microsensor concept based on interfacial liquid–liquid microwave flow in a microfluidic channel. Journal of Micromechanics and Microengineering 15, 2326–2338.

Anczykowski, B., Cleveland, J., Krüger, D., Elings, V., Fuchs, H., 1998. Analysis of the interaction mechanisms in dynamic mode SFM by means of experimental data and computer simulation. Applied Physics A. Materials Science and Processing 66, 885–889.

Binnig, G., Quate, C., Gerber, C., 1986. Atomic force microscope. Physical Review Letters 56, 930–933.

Burg, T., Manalis, S., 2003. Suspended microchannel resonators for biomolecular detection. Applied Physics Letters 83 (13), 2698–2700.

Butt, H.J., Siedle, P., Seifert, K., Fendler, K., Seeger, T., Bamberg, E., Weisenhorn, A., Goldie, K., Engel, A., 1993. Scan speed limit in atomic force microscopy. Journal of Microscopy 169, 75–84.

Chen, G.Y., Warmack, R.J., Thundat, T., Allison, D., Huang, A., 1994. Resonance response of scanning force microscopy cantilevers. Review of Scientific Instruments 65 (8), 2532–2537.

Chen, J., Darhuber, A., Troian, S., Wagner, S., 2004. Capacitive sensing of droplets for microfluidic devices based on thermocapillary actuation. Lab on a Chip 4, 473–480.

Hauptmann, P., 1991. Resonant sensors and applications. Sensors and Actuators A 25–27, 371–377.

Inaba, S., Akaishi, K., Mori, T., Hane, K., 1993. Analysis of the resonance characteristics of a cantilever vibrated photothermally in a liquid. Journal of Applied Physics 73 (6), 2654–2658.

Jakoby, B., Scherer, M., Buskies, M., Eisenschmid, H., 2003. An automotive engine oil viscosity sensor. IEEE Sensor Journal 3 (5), 562–568.

Kedzierski, M.A., 2003. Microchannel heat transfer, pressure drop and macro prediction methods. In: Proceedings of 2nd International Conference on Heat Transfer, Fluid Mechanics and Thermodynamics (HEFAT2003).

Li, Y.-C., Ho, M.-H., Hung, S.-J., Chen, M.-H., Lu, M.S.-C., 2006. CMOS micromachined capacitive cantilevers for mass sensing. Journal of Micromechanics and Microengineering 16, 2659–2665.

Martin, S., Frye, G., Wessendorf, K., 1994. Sensing liquid properties with thickness-shear mode resonators. Sensors and Actuators A 44, 209–218.

Naik, T., Longmire, E., Mantell, S., 2003. Dynamic response of a cantilever in liquid near a wall. Sensors and Actuators A 102, 240–244.
Oden, P., Chen, G.Y., Steele, R.A., Warmack, R.J., Thundat, T., 1996. Viscous drag measurements utilizing microfabricated cantilevers. Applied Physics Letters 68 (26), 3184–3186.
Pan, F., Kubby, J., Peeters, E., Tran, A., Mukherjee, S., 1998. Squeeze film damping effect on the dynamic response of a MEMS torsion mirror. Journal of Micromechanics and Microengineering 8, 200–208.
Patois, R., Vairac, P., Cretin, B., 2000. Near-field acoustic densimeter and viscosimeter. Review of Scientific Instruments 71 (10), 3860–3863.
Rey, A., 2000. Modeling the Wilhelmy surface tension method for nematic liquid crystals. Langmuir 16, 845–849.
Seo, J.H., Brand, O., 2005. Novel high q-factor resonant microsensor platform for chemical and biological applications. In: The 13th International Conference on Solid State Sensors, Actuators and Microsystems, pp. 593–596.
Smits, J., 1990. Piezoelectric micropump with three valves working peristaltically. Sensors and Actuators A21–A23, 203–206.
Tamayo, J., Humphris, A., Malloy, A., Miles, M., 2001. Chemical sensors and biosensors in liquid environment based on microcantilevers with amplified quality factor. Ultramicroscopy 86, 167–173.
Timoshenko, S., 1984. Strength of Materials. Krieger.
Van Lintel, H.T.G., Van de Pol, F.C.M., Bouwstra, S., 1988. A piezoelectric micropump based on micromachining of silicon. Sensors and Actuators 15, 153–167.
Veijola, T., Kuisma, H., Lahdenperä, J., Ryhänen, T., 1995. Equivalent-circuit model of the squeezed damped film in a silicon accelerometer. Sensors and Actuators A 48, 239–248.
Veijola, T., Pursula, A., Raback, P., 2005. Extending the validity of existing squeeze damper models with elongations of surface dimensions. Journal of Micromechanics and Microengineering 15, 1624–1636.
Walters, D.A., Cleveland, J.P., Thomson, N.H., Hansma, P.K., Wendman, M.A., Gurley, G., Elings, V., 1996. Short cantilevers for atomic force microscopy. Review of Scientific Instruments 67 (10), 3583–3590.
Yi, J., Shih, W., Mutharasan, R., Shih, W.-H., 2003. In-situ cell detection using piezoelectric lead zirconate titanate-stainless steel cantilevers. Journal of Applied Physics 93 (1), 619–625.
Zhang, H., Kim, E.S., 2003. Vapor and liquid mass sensing by micromachined acoustic resonator. In: IEEE 16th Annual International Conference on MEMS, pp. 470–473.